Ionics (2023) 29:3759–3767
https://doi.org/10.1007/s11581-023-05138-0

ORIGINAL PAPER

Fabrication of Ag nanoparticles decorated on the NiAl-oxide@PPy for non-enzymatic H_2O_2 sensing

Wei Yan[1] · Hong-Yan Zeng[1] · Kai Zhang[1] · Kai-Min Zou[1]

Received: 14 March 2023 / Revised: 10 June 2023 / Accepted: 20 July 2023 / Published online: 2 August 2023

Abstract

The NiAlO@PPy-Ag sensing material was designed and prepared via *in-situ* oxidative polymerization of pyrrole monomer on the NiAl-oxide (NiAlO), and then anchoring Ag nanoparticles (NPs) on the surface of the NiAlO@PPy carrier. It was determined that the NiAlO particles were encased by PPy chains and Ag NPs were homogeneously distributed on the NiAlO@PPy based on various structural characterization. Subsequently, the NiAlO@PPy-Ag was directly fabricated into a non-enzymatic sensor for the detection of H_2O_2, which sensor showed a high sensitivity and selectivity toward H_2O_2 with a low detection limit of 0.03 μmol•L^{-1} and high sensitivity of 346.50 μA•$mmol^{-1}$•cm^{-2}, and excellent repeatability and reproducibility. The results demonstrated that the NiAlO@PPy-Ag was a promising electrocatalytic material for H_2O_2 detection in the biological, clinical and environmental fields.

Keywords NiAl-oxide · Polypyrrole · Silver nanoparticles · Non-enzymatic sensor · H_2O_2 detection

Introduction

Electrochemical biosensors, especially enzymatic sensor, have attracted much attention due to simplicity, high selectivity and sensitivity. However, the application of enzymatic sensors is limited because of high cost, complicated immobilization procedure and limited stability. Non-enzyme electrocatalytic materials are developed to avoid the issues [1–3]. All kinds of efforts have been used to improve the performances of non-enzyme sensor materials [4, 5]. Especially, Ni-based metal oxides have attracted enormous interest recently for the sensor research and practical application such as the detections of H_2O_2 [6, 7], glucose [4, 8] and uric acid [9], due to natural abundance, good biological compatibility and high electron transfer capability. For example, NiO anchored on carbon nanofibers displayed a good electrocatalytic activity towards H_2O_2 with a low detection limit (LOD) of 0.57 μmol•L^{-1} and high sensitivity of 304.2 μA•mol•L^{-1}•cm^{-2} [10]. The non-enzyme sensor based on NiCoP displayed a good electrochemical sensing property with a LOD of 1.190 μmol•L^{-1} and selectivity 225.7 μA•mol•L^{-1}•cm^{-2} toward H_2O_2 [11]. Nevertheless, it still faces the challenge of improving the stability and selectivity in applications of non-enzyme sensor.

Incorporating conducting polymers with the Ni-based metal oxides gives a promising way to strengthen the electrochemical sensing performances, in which conducting polymers can prevent the aggregation of metal oxides in favor of the electron transfer to increase the sensitivity and selectivity [12, 13]. Among the polymers, polypyrrole (PPy) as excellent electron donor is one of the most favorable conducting polymers due to flexible, ease of synthesis and high conductivity, which make it an interesting matrix for the organic-inorganic composites [14–16]. It is believed that the incorporation of the Ni-based metal oxides with PPy are expected to display new properties over their single component, making them potential for non-enzymatic sensor application. Moreover, Ag nanoparticles (NPs), as attractive non-enzymatic alternative, were decorated on the organic-inorganic composites can further enhance the electrocatalytic activity for the detection of H_2O_2 [17, 18].

In the present work, the NiAlO@PPy-Ag was synthesized by the incorporation of NiAl-oxide (NiAlO) and PPy together with the anchoring of Ag NPs, and used toward the detection of H_2O_2. To the best of our knowledge, little research is reported on the use of NiAlO@PPy-Ag as a sensor material for the detection of H_2O_2. The structure,

✉ Hong-Yan Zeng
hongyanzeng99@hotmail.com

[1] College of Chemical Engineering, Xiangtan University, Xiangtan 411105, Hunan, China

morphology and electrochemical properties of the as-prepared samples were determined using various characterization techniques and electrochemical measurements. As a non-enzymatic H_2O_2 sensor material, the NiAlO@PPy-Ag exhibited superior sensing performances with a relatively wide potential range, high sensitivity and good stability.

Experimental

Materials

In the experiments, all reagents were of analytical grade without any further purification. 0.1 mol•L^{-1} phosphate buffer solution (PBS) with pH 7.0 was prepared by dissolving KH_2PO_4 and K_2HPO_4 in distilled water, and distilled water was used to prepare all the solutions. A pH electrode (Mettler Toledo 5-2C) was used for pH measurements.

Preparation of substrate materials

The NiAl-oxide was prepared by urea method (urea/NO_3^- molar ratio of 4.0). In brief, $Ni(NO_3)_2{\cdot}6H_2O$ and $Al(NO_3)_3{\cdot}9H_2O$ (Ni^{2+} + Al^{3+} = 0.30 mol·L^{-1}, Ni/Al molar ratio of 3.0) as well as urea were dissolved in distilled water under vigorous stirring at 105°C for 12 h, and then filtered, washed, and dried at 80°C for 24 h. The resulting product was calcined in air atmosphere at 400°C for 4 h, which was denoted as NiAlO.

The NiAlO (0.1 g·L^{-1}) was immersed in the solution containing 0.1 g·L^{-1} sodium anthraquinone disulfonate as dopant under stirring in an ice bath for 15 min. 9.0 mL·L^{-1} pyrrole monomer was added and maintained for 30 min under stirring, and then the $FeCl_3$ (initiator) solution (3.2 mL·L^{-1}) was added dropwise into the reaction vessel to initiate the polymerization of pyrrole at 0~4°C for 6 h. The precipitate was filtered, washed and dried at 60°C for 24 h, which was denoted as NiAlO@PPy. For comparison, the pure polypyrrole (PPy) was also prepared through the above-mentioned process in the absence of the NiAlO.

In our preliminary tests, it was found that the optimized $AgNO_3$ amount was 0.17 mass ratio of $AgNO_3$ to NiAlO@PPy (seeing detailed information in Fig. S1). So, $AgNO_3$ with 0.17 mass ratio of $AgNO_3$ to NiAlO@PPy was dissolved in the NiAlO/PPy suspension under stirring, and then $NaBH_4$ solution was mixed dropwise (0.5 molar ratio of $AgNO_3$ to $NaBH_4$) under stirring for 2 h. After reaction, the resulting product was centrifuged and washed thoroughly, and dried at 60°C overnight, which was denoted as NiAlO@PPy-Ag. The preparation process of the NiAlO, NiAlO@PPy and NiAlO@PPy-Ag are illustrated in Scheme 1.

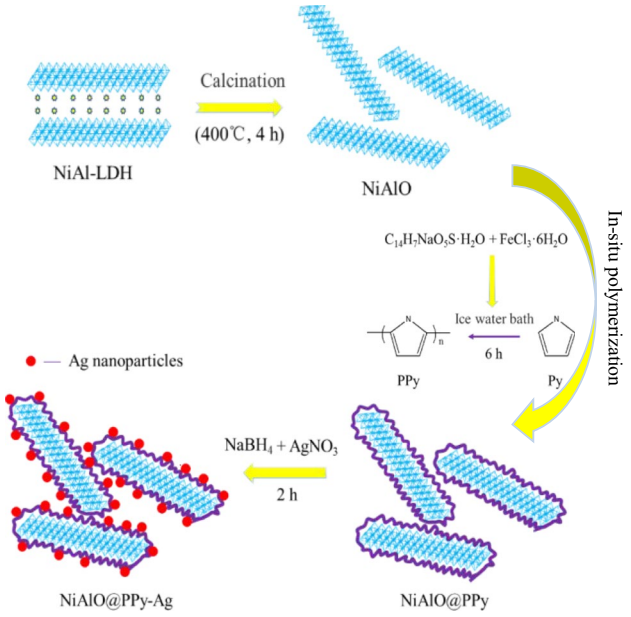

Scheme 1 Schematic preparation process of NiAlO@PPy-Ag

Characterization

X-ray diffraction (XRD) patterns were collected on a Rigaku D/max-2550PC (λ=1.5406 Å) with Cu Kα radiation. The morphology was investigated by scanning electron microscopy (SEM, JEOL JSM-6700F) and transmission electron microscopy (TEM, JEM2100). The X-ray photoelectron spectroscopy (XPS) was carried out by Thermo Fisher Scientific K-Alpha. The composition was characterized by energy-dispersive spectrometry (EDS, Noran SystemSix).

Electrochemical measurements

The substrate material films were immobilized on bare glassy carbon electrodes (GCE). Before immobilization, the GCE with a diameter of 2.0 mm was pretreated according to the literature [19]. The active substance was dispersed in distilled water under ultrasonic treatment, and then the 10 μL dispersion solution containing 1.0 g·L^{-1} active substance was dropped onto the pretreated GCE. After immobilization, the electrode was washed in distilled water and then dried under infrared radiation for 5 min to obtain the modified electrodes. The electrodes modified by the NiAlO, PPy, NiAlO@PPy and NiAlO@PPy-Ag were designated as NiAlO/GCE, PPy/GCE, NiAlO@PPy/GCE and NiAlO@PPy-Ag/GCE, respectively.

All electrochemical experiments were performed on a CHI660D electrochemical workstation (Shanghai Chenhua Apparatus Co. Ltd., Shanghai, China) with working

electrode, a platinum plate counter electrode and a saturated calomel electrode (SCE). The electrolyte was 0.1 mol•L^{-1} KCl solution containing 5 mmol·L^{-1} $K_3[Fe(CN)_6]$ and 5 mmol•L^{-1} $K_4[Fe(CN)_6]$. CV measurements were performed between −0.2 and 0.6 V at the 12th cycle. EIS was between 0.01 and 100 KHz under open circuit voltage conditions. All experiments were carried out at room temperature. The H_2O_2 limit of detection (LOD, μmol·L^{-1}) was calculated as follows [20],

$$LOD = 3_{s_B}/m \quad (1)$$

where s_B was the standard deviation of blank test, and m was slope of calibration curve.

Results and discussion

Characterization of the as-prepared samples

Fig. 1 shows the XRD patterns of the NiAlO, pure PPy, NiAlO@PPy and NiAlO@PPy-Ag, where a broad reflection at 25.5° in the pure PPy was due to the aligned polypyrrole chains at the interplanar spacing of protonated PPy [15]. The NiAlO displayed the (111), (200), (220) and (311) planes attributing to NiO (JCPDS no. 65-5745) [5], where no Al_2O_3 phase was detected with the idea that Al^{3+} formed amorphous phases or dispersed into the NiO matrix [21]. The NiAlO@PPy clearly exhibited the coexistent presence of the characteristic reflections of NiO and PPy, suggesting that the coating of PPy had no impact on the crystallinity of the NiAlO. In the XRD pattern of the NiAlO@PPy-Ag, the new reflections

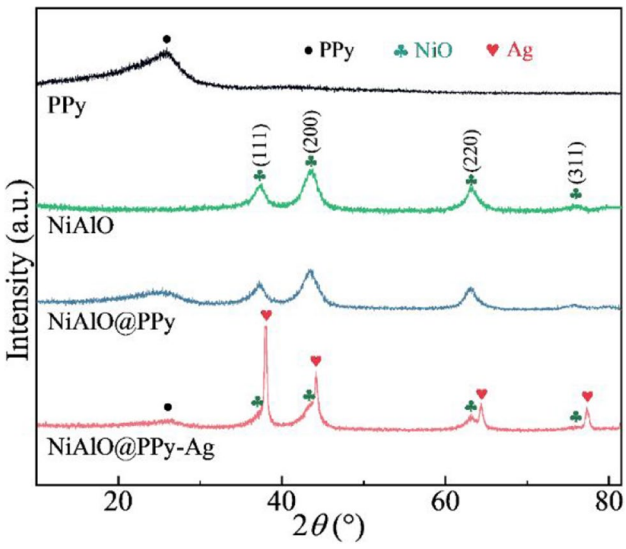

Fig. 1 XRD patterns of the NiAlO, pure PPy, NiAlO@PPy and NiAlO@PPy-Ag

at 38.0, 45.2, 64.4 and 77.3° corresponding to (111), (200), (220), and (311) planes of metallic Ag^o (JCPDS no. 04-0783) besides the crystal phases of NiO and PPy, showing that Ag^o NPs were anchored on the NiAlO@PPy [22].

The morphology of the NiAlO, pure PPy, NiAlO@PPy and NiAlO@PPy-Ag were observed by SEM. As seen in Fig. 2, the NiAlO demonstrated a flower-like layer structure consisting of individually layered platelets, while the pure PPy showed platy particles with average diameter about 0.6 μm. After coating PPY on the NiAlO NPs, the NiAlO@PPy particles still showed individually layered platelets, but the platelets tended to aggregate into cluster. The PPy chains acting as binders glued together with the NiAlO particles, which provided many active sites for the electrochemical reaction [23]. Clearly, Ag^o NPs (white arrow) were dispersed on the NiAlO@PPy-Ag, indicating that the metallic Ag^o NPs were anchored on the NiAlO@PPy-Ag surface. Furthermore. the TEM image ascertained that the presence of metallic Ag^o and PPy, in which the Ag^o NPs were anchored at the NiAlO nanoparticles (in dark), and PPy (in gray), as pointed by the white arrows (Fig. S2).

The elemental composition and surface state of the NiAlO@PPy-Ag were examined by XPS, and the results are shown in Fig. S3. The high-resolution Ni 2p spectrum appeared two main peaks at 873.3 eV (Ni $2p_{1/2}$) and 855.7 eV (Ni $2p_{3/2}$) with a spin-energy separation of 17.6 eV, suggesting a typical feature of the Ni^{2+} in the NiAlO [24]. the O 1s spectrum could be fitted into three peaks, which peaks at 531.4 eV was related to hydroxyl radical (−OH), and the other two peaks were assigned to lattice oxygen (O_l, Ni-O, Al-O, Ag-O) [25, 26]. The fitting N 1s spectrum presented three existence forms, corresponding to $-N^+H-$ (402.3 eV), –NH– (400.2 eV) and =NH– (398.4 eV) [15], respectively. The Ag 3d spectrum had two individual peaks corresponding to Ag $3d_{3/2}$(374.2 eV) and Ag $3d_{5/2}$ (368.1 eV), which were attributed to metallic Ag^o [15]. In the deconvoluted C1s spectrum, three peaks at 288.5, 286.2, and 284.8 eV belonged to the C=O, C-N and C-C/C=C groups [27], respectively. Finally, the Al 2p spectrum showed a peak at 72.4 eV, which was relating to the Al^{3+} species (Al-O) [28]. Furthermore, the elemental composition of the NiAlO@PPy-Ag was further verified by EDS, and the EDS results are shown in Table S1. As seen in Table S1 and Fig. S4, the NiAlO@PPy contained Ni, Al, C, O, N, Cl and S elements, while the Ag element (1.43% atomic content) was detected in the NiAlO@PPy-Ag except the elements in the NiAlO@PPy. The Cl atoms in the NiAlO@PPy and NiAlO@PPy-Ag were from initiator $FeCl_3$, and S atoms should derive from the dopant sodium anthraquinone disulfonate during the polymerization of pyrrole monomer [29]. The XPS and EDS results supported the point from the XRD and SEM/TEM that Ag NPs was successfully anchored onto the NiAlO@PPy, in which PPy was coated on the surface of the NiAlO.

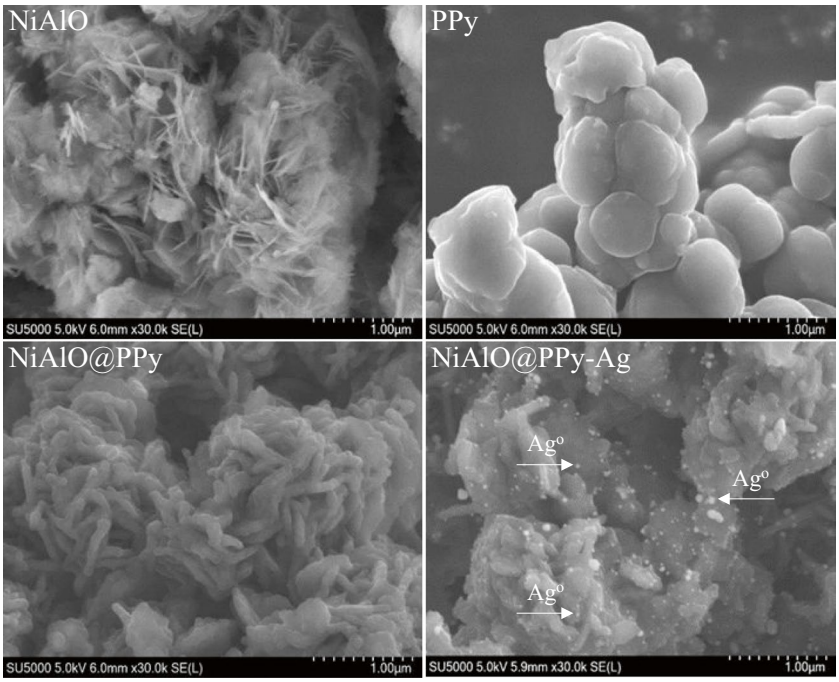

Fig. 2 SEM images of the NiAlO, pure PPy, NiAlO@PPy and NiAlO@PPy-Ag

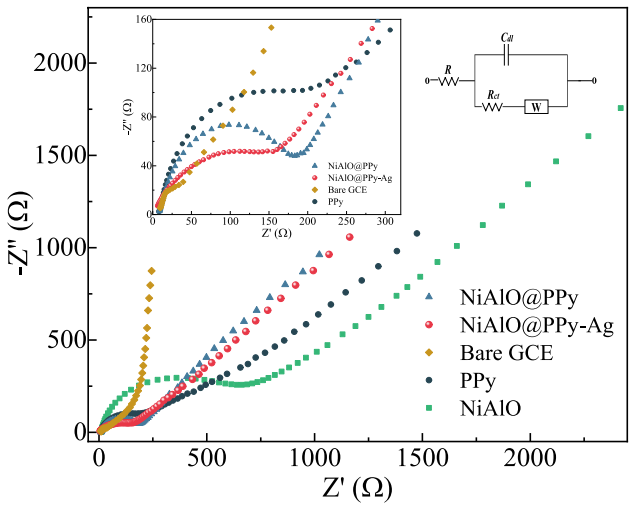

Fig. 3 Nyquist plots of the bare GCE, NiAlO, pure PPy, NiAlO@PPy and NiAlO@PPy-Ag

Electrochemical performances of the substrate materials

To explore their potential application in electrochemical sensor devices, the electrochemical properties of the NiAlO, pure PPy, NiAlO@PPy and NiAlO@PPy-Ag were investigated by EIS (Fig. 3). The Nyquist curve of the bare GCE displayed a very small semicircle domain, implying a very low electron transfer resistance. The charge-transfer resistance (R_{ct}) were calculated by fitting the EIS data to the suitable equivalent circuit (Fig. 3 inset, Chi square values $\leq 1.20\times10^{-2}$). The sequence order of the R_{ct} values was NiAlO/GCE (528.10 Ω) > PPy/GCE (173.50 Ω) > NiAlO@PPy/GCE (128.90 Ω) > NiAlO@PPy-Ag/GCE (90.53 Ω) > GCE (0.02 Ω). The hindered electron transfer for the NiAlO/GCE was caused by intrinsic poor electroconductivity. It was found that the R_{ct} value markedly decreased after coating conductive polymer PPy on the NiAlO surface, and further fell after the anchoring of Ag NPs, revealing that the coating of PPy together with anchoring of Ag NPs could improve the electrical conductivity, namely the NiAlO@PPy-Ag/GCE had the fastest electron-transfer kinetics.

The electrochemical activity of the NiAlO, pure PPy and NiAlO@PPy-Ag was investigated, which displayed an apparent couple of reversible redox peaks in Fig. 4. As shown in Fig. 4 inset, the CV curves of the NiAlO/GCE and pure PPy/GCE at 10 $mV{\cdot}s^{-1}$ for 12 cycles exhibited a very weak current response, revealing a sluggish redox reaction kinetics and low sensitivity. When the NiAlO@PPy-Ag was immobilized on GCE, the current response in the system signifcantly increased, showing an enhanced sensitivity. Furthermore, the CV behavior of the NiAlO@PPy-Ag was evaluated at different scan rates (Fig. 4). The shape of the CV curves remained nearly constant at different scan rates, and the peak currents increased rose with rising the scan rate from 10 to 150 $mV{\bullet}s^{-1}$, suggesting a good reversibility. The peak currents were linearly related to the square root of scan rate with high correlation coefficients ($R^2 \geq 0.9589$, Fig. 4 inset), indicating that the electron transfer reaction in the NiAlO@PPy-Ag was a diffusion-controlled process [30].

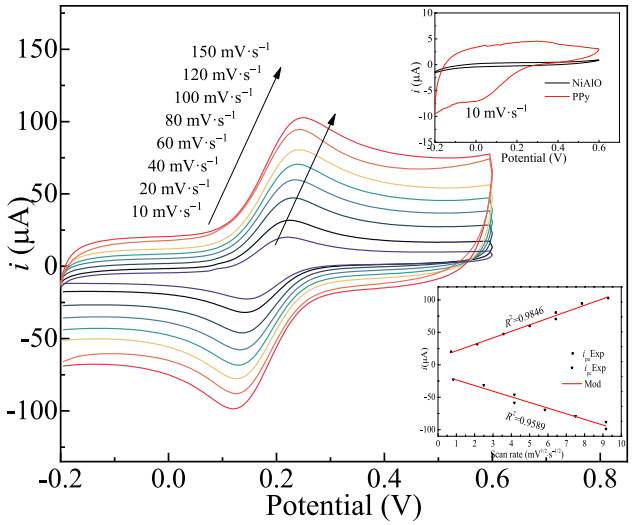

Fig. 4 CV curves of the NiAlO@PPy-Ag at different scan rates and plots (inset) of the peak current vs. square root of scan rate

Electrocatalysis of the NiAlO@PPy-Ag towards H_2O_2

Electroactivity of the NiAlO@PPy/GCE and NiAlO@PPy-Ag/GCE towards the reduction of H_2O_2 were determined by CV and amperometric detection in 0.1 mol•L^{-1} PBS solution (pH 7.0) at the 12th cycle, and the results are shown in Fig. 5. As seen in Fig. 5A inset, the NiAlO@PPy/GCE showed no reduction activity towards H_2O_2 in the reaction system containing 7.0 mmol•L^{-1} H_2O_2. Interestingly, the cathodic peak current in the CV curves increased dramatically with increasing H_2O_2 concentration from 0 to 7.0 mmol•L^{-1} at the. The result uncovered that Ag NPs played a key role in the H_2O_2 reduction, which endowed the NiAlO@PPy-Ag/GCE a high electrocatalytic performance toward the H_2O_2 reduction. On the other hand, the amperometric response of the NiAlO@PPy/GCE and NiAlO@PPy-Ag/GCE upon the successive addition of H_2O_2 in 0.1 mol•L^{-1} PBS solution (pH=7.0) at −0.3 V was evaluated under stirring (Fig. 5B). The NiAlO@PPy/GCE was no response to H_2O_2, implying a low electrochemical response towards H_2O_2. On the contrast, the NiAlO@PPy-Ag showed a typical current-time (*i*-*t*) plot upon the successive addition of H_2O_2, and the amperometric response current increased with the adding of H_2O_2, indicating an excellent electrocatalytic activity to H_2O_2. So, the NiAlO@PPy-Ag/GCE was chosen as a sensor to detect H_2O_2 by Amperometric determination.

Optimization of amperometric determination

In order to ensure the performance of the NiAlO@PPy-Ag sensor, the effect of some parameters (active substance loading, applied potential and pH) were investigated by amperometric detection in the PBS solution containing 2.0 mmol•L^{-1} of H_2O_2. Firstly, the effect of NiAlO@PPy-Ag loading on the amperometric response in initial pH 7.0 at −0.3 V (300 rpm) is shown in Fig. 6A, where a given volume of the suspension containing 1.0 g·L^{-1} NiAlO@PPy-Ag was dropped onto the GCE. The amperometric response increased obviously with the loading from 1 to 5 μL, and then decreased. Thus, 5 μL suspension was selected for the amperometric detection of H_2O_2. Second, the applied potential was studied at initial pH 7.0 in the range of −0.5 to 0.1 V. As seen in Fig. 6B, the amperometric response reached the highest above or equal to −0.3 V, and so the potential was determined to be−0.3 V as the applied potential. At a low potential, the background current decreased and the response toward the active substance was weakened, leading to the lessening in the reduction current [31]. Finally, initial pH in the detecting system was evaluated at −0.3 V (300 rpm) (Fig. 6C). The current response increased gradually with initial pH, and then achieved the maximum at pH 7.0. So, initial pH 7.0 in the PBS solution was selected for amperometric detection of H_2O_2.

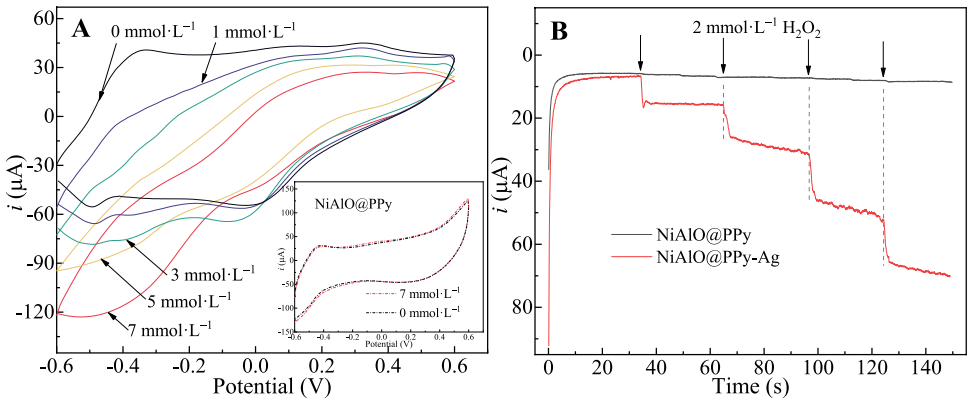

Fig. 5 CV and current-time curves of the NiAlO@PPy-Ag in the PBS solution containing H_2O_2

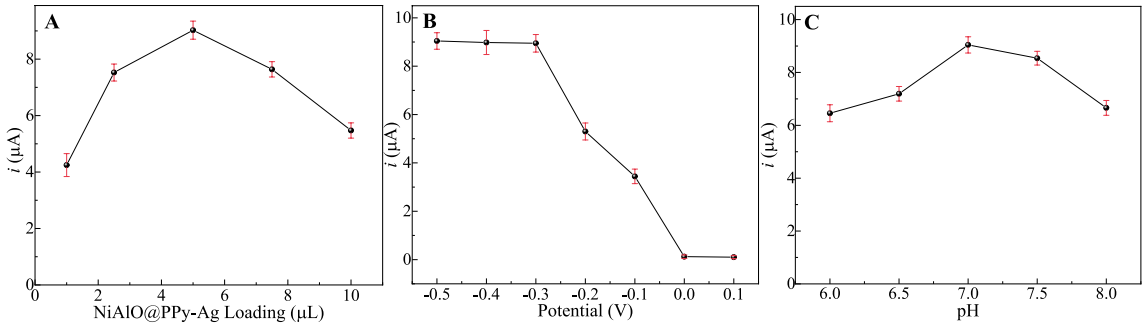

Fig. 6 Effect of active substance loading (**A**), applied potential (**B**) and pH (**C**) on the amperometric response

Amperometric detection toward H_2O_2

The sensitivity of the NiAlO@PPy-Ag/GCE towards H_2O_2 was determined by amperometric detection at −0.3 V, where a typical steady-state *i-t* response plot with continuous addition of H_2O_2 every 30 s is shown in Fig. 7. As expected, well-defined stepwise increment in the amperometric response was observed upon the addition of H_2O_2. The sensor reached the steady-state current within 3 s, suggesting very fast response process in the NiAlO@PPy-Ag/GCE. The sensor had a wide linear range from 1.0×10^{-2} to 8.0 mmol·L^{-1} (R^2 0.998, Fig. 7 inset), and the sensitivity was estimated to be 346.50 μA·mmol^{-1}·cm^{-2} with the detection limit (LOD) of 0.03 μmol·L^{-1} (S/N=3).

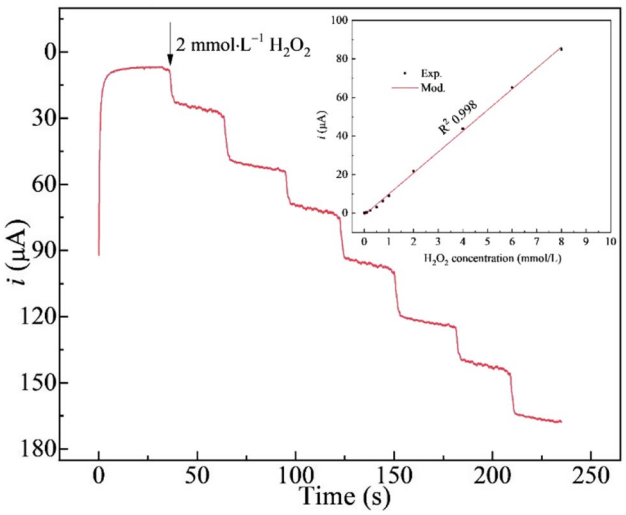

Fig. 7 Amperometric response of the NiAlO@PPy-Ag sensor on successive injection of H_2O_2 and corresponding calibration curve (inset) of the response current (i) versus H_2O_2 concentration

Furthermore, the analytical performance of the H_2O_2 sensor were compared with some other non-enzymatic H_2O_2 sensors reported in the literature [5–7, 10, 11, 39–44]. As listed in Table 1, analytical performance of the present NiAlO@PPy-Ag sensor was comparable to those of the H_2O_2 sensors.

The repeatability, reproducibility and stability of the as-prepared NiAlO@PPy-Ag/GCE were studied in 1.0 mmol·L^{-1} initial H_2O_2 concentration. Six successive amperometric detections were carried out to investigate the repeatability, where the response current (*i*) were 8.79, 8.92, 9.25, 9.15, 8.86 and 9.08 μA, respectively. The relative standard deviation (RSD) was found to be 1.99%, which indicated a satisfactory precision. Furthermore, six different modified sensors were prepared under the same condition, where the response current to the different electrodes were 8.86, 8.95, 9.06, 9.15, 9.10 and 8.93 μA, respectively. The RSD was 1.24%, confirming that the NiAlO@PPy-Ag/GCE could be reproducible. In order to investigate the stability, the sensor was stored in ambient condition and monitored over a period of 30 days. After 1 week, only 1.5% of the current signal was lost, 3.4% of the lost after 2 weeks, and maintained around 91.3% of the initial current signal for over 1 month. In a word, the results indicated that the NiAlO@PPy-Ag/GCE had a good repeatability, reproducibility and stability.

The influence of common interfering species on the analytical performance of the NiAlO@PPy-Ag/GCE was also evaluated. The amperometric response of the sensor toward addition of 1.0 mmol·L^{-1} H_2O_2 and succeeding NaCl, KCl, glucose, uric acid, ascorbic acid and dopamine (each 10 mmol·L^{-1}) in a 0.1 mol·L^{-1} PBS solution (pH 7.0) was determined (Fig. 8). As seen in Fig. 8, the *i-t* responses of the mentioned interfering substance were quite negligible, demonstrating that the NiAlO@PPy-Ag sensor had a superior selectivity towards H_2O_2.

Table 1 Comparison with the analytical performance of other sensors for H_2O_2 detection

	LOD ($\mu mol \cdot L^{-1}$)	Linear range ($\mu mol \cdot L^{-1}$)	Sensitivity ($\mu A \cdot mmol^{-1} \cdot cm^{-2}$)	Reference
NiO-NSs/CF-1801*	0.01303	200-2750	23.30	[5]
Ni/NiO@C	0.9	10-80700	32.09	[6]
GCE/Nafion/Ni	1.8	5-500	-	[7]
CNFs/NiO*	0.57	0.1-3489.9	304.2	[10]
NiCoP	1.190	50-4000	225.7	[11]
LSG-Ag*	7.9	100-10000	32	[32]
$Cu_2O@Cu_9S_5$	0.02882	0.1-3500	299.74	[33]
Cu_2O/BiOI	0.44	1.99-17540	213.87	[34]
$ZnMn_2O_4$	0.13	20-15000	277100	[35]
Fe-NGCs*	0.53	1-5000	184.4	[36]
NiO-PE(A4)*	5	-	25	[37]
NiAlO@PPy-Ag	0.03	10-8000	346.5	This work

*: NSs/CF-1801: nanosheets/carbon foam-180°C for 1 h; CNFs: carbon nanofibers; LSG: laser scribed graphene; NGCs: N-doped graphitic nanocages; PE(A4): plastic electrode (triethylamine, 400°C)

Practicality of the sensor

To evaluate the possible applicability of the present sensor, the determination of H_2O_2 in the water samples from different sources was investigated. The standard addition method was used, for no response towards H_2O_2 was found in the water samples. The collected water samples were diluted using 0.1 $mmol \cdot L^{-1}$ PBS solution (pH 7.0) before the determinations, and all the determinations were carried out four times in parallel. As shown in Table 2, the calculated recovery and RSD indicated that the present NiAlO@PPy-Ag sensor had an appreciable practicality in the determination of H_2O_2.

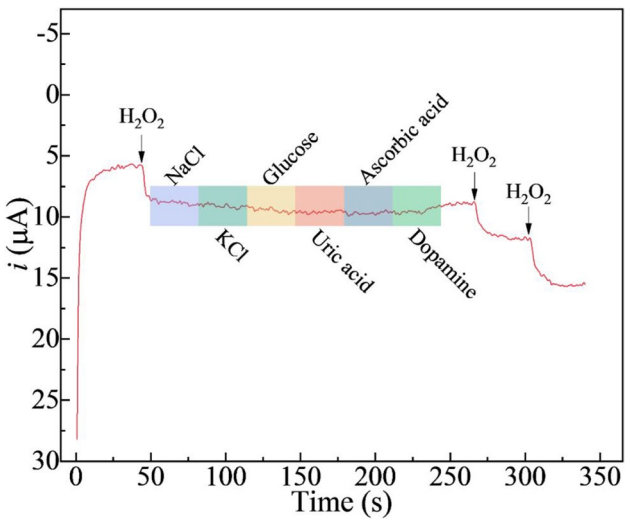

Fig. 8 Amperometric response of the NiAlO@PPy-Ag sensor to successive addition of H_2O_2 and the interfering substances at −0.3 V

Conclusions

The NiAlO@PPy-Ag material was successfully prepared via *in-situ* oxidative polymerization of pyrrole monomer on the NiAl-oxide (NiAlO), and then anchoring Ag nanoparticles (NPs) on the surface of the NiAlO@PPy carrier. The presence of Ag NPs and PPy was confirmed by XRD, EDS and SEM techniques. Such the architectures not only had respective merits of each component, but also showed a strong synergistic effect among the NiAlO, PPy and Ag^o, where the PPy shell provided more anchoring sites for Ag^o, and Ag NPs had excellent electrocatalytic reduction ability to H_2O_2 resulting in high response towards H_2O_2. The present @PPy-Ag sensor demonstrated an attractively electrocatalytic activity in the H_2O_2 reduction, which showed a wide linear detection range, low LOD, and high sensitivity. Furthermore, the sensor was also practically applied to determine H_2O_2 in the water samples from different sources. The present work provided

Table 2 Analytical results for H_2O_2 in real water samples

Samples	Added ($mmol \cdot L^{-1}$)	Found * ($mmol \cdot L^{-1}$)	RSD (%)	Recovery ** (%)
River water	0.50	0.487	3.04	97.35
	1.00	0.960	1.98	95.98
Pond water	0.50	0.491	4.09	98.20
	1.00	0.974	2.23	97.40
Tap water	0.50	0.480	2.89	96.00
	1.00	0.978	1.60	97.80

*Mean of four measurements

**Relative standard deviation for n = 4

a low cost, simple preparation, environmental friend and green synthetic method to prepare the NiAlO@PPy-Ag material, which had a great potential commercial application for H_2O_2 detection.

Supplementary Information The online version contains supplementary material available at https://doi.org/10.1007/s11581-023-05138-0.

Author contributions Wei Yan: Writing - review & editing, Software. Hong-Yan Zeng: Conceptualization, Methodology, Supervision. Kai Zhang: Data curation, Validation, Visualization. Kai-Min Zou: Writing - original draft preparation, Investigation.

Data availability The authors do not have the permission to share data.

Declaration

Competing Interest The authors declare that they have no known conflict of financial interests or personal relationships that could have appeared to influence the content reported in this paper.

References

1. Dong Q, Ryu H, Lei Y (2021) Metal oxide based non-enzymatic electrochemical sensors for glucose detection. Electrochim Acta 370:137744
2. Yang X, Qiu P, Yang J, Fan Y, Wang L, Jiang W, Cheng X, Deng Y, Luo W (2021) Mesoporous materials-based electrochemical biosensors from enzymatic to nonenzymatic. Small 17(9):1904022
3. Thatikayala D, Ponnamma D, Sadasivuni KK, Cabibihan J-J, Al-Ali AK, Malik RA, Min B (2020) Progress of advanced nanomaterials in the non-enzymatic electrochemical sensing of glucose and H_2O_2. Biosensors 10(11):151
4. Rafique N, Hannan Asif A, Hirani RAK, Wu H, Shi L, Zhang S, Sun H (2022) Binder free 3D core-shell NiFe layered double hydroxide (LDH) nanosheets (NSs) supported on cu foam as a highly efficient non-enzymatic glucose sensor. J Colloid Interface Sci 615:865–875
5. Liu M, An M, Xu J, Liu T, Wang L, Liu Y, Zhang J (2021) Three-dimensional carbon foam supported NiO nanosheets as non-enzymatic electrochemical H_2O_2 sensors. Appl Surf Sci 542:148699
6. Ma X, Tang K, Yang M, Shi W, Zhao W (2021) Metal-organic framework-derived yolk-shell hollow Ni/NiO@C microspheres for bifunctional non-enzymatic glucose and hydrogen peroxide biosensors. J Mater Sci 56(1):442–456
7. Islam MDF, Islam MT, Hasan MM, Rahman MM, Nagao Y, Hasnat MA (2022) Facile fabrication of GCE/Nafion/Ni composite, a robust platform to detect hydrogen peroxide in basic medium via oxidation reaction. Talanta 240:123202
8. Xiao L, Yang K, Duan J, Zheng S, Jiang J (2022) The nickel phosphate rods derived from Ni-MOF with enhanced electrochemical activity for non-enzymatic glucose sensing. Talanta 247:123587
9. Azeredo NFB, Gonçalves JM, Rossini PO, Araki K, Wang J, Angnes L (2020) Uric acid electrochemical sensing in biofluids based on Ni/Zn hydroxide nanocatalyst. Microchim Acta 187(7):379
10. Cai J, Vasudevan SV, Wang M, Mao H, Bu Q (2022) Microwave-assisted synthesized renewable carbon nanofiber/nickel oxide for high-sensitivity detection of H_2O_2. Electroanal Chem 924:116876
11. Wang Z-Y, Chang H-W, Tsai Y-C (2023) Synthesis of bimetallic Ni-Co phosphide nanosheets for electrochemical non-enzymatic H_2O_2 sensing. Nanomaterials 13(1):66
12. John L, Benny AR, Cherian SY, Narahari A, Varghese A, Hegde G (2021) Electrochemical sensors using conducting polymer/noble metal nanoparticle nanocomposites for the detection of various analytes: a review. J Nanostruct Chem 11(1):1–31
13. Emir G, Dilgin Y, Ramanaviciene A, Ramanavicius A (2021) Amperometric nonenzymatic glucose biosensor based on graphite rod electrode modified by Ni-nanoparticle/polypyrrole composite. Microchem J 161:105751
14. Jain R, Jadon N, Pawaiya A (2017) Polypyrrole based next generation electrochemical sensors and biosensors: a review. TrAC Trends Anal Chem 97:363–373
15. Sun R, Zhang W, Zhang J, Zhao Y, Yuan H, Guan H, Huang C, Ma C, Ge J, Tian W, Hao L (2023) Flexible and conductive polypyrrole/Ag/cellulose paper bar with sensitive response to multiple stimulus of pH, mist, breath and finger press. Mater Lett 341:134260
16. Rizi KS, Hatamluyi B, Rezayi M, Meshkat Z, Sankian M, Ghazvini K, Farsiani H, Aryan E (2021) Response surface methodology optimized electrochemical DNA biosensor based on HAPNPTs/PPY/MWCNTs nanocomposite for detecting mycobacterium tuberculosis. Talanta 226:122099
17. Shafa M, Ahmad I, Hussain S, Asif M, Pan Y, Zairov R, Alothman AA, Ouladsmane M, Ullah Z, Ullah N, Lai C, Jabeen U (2023) Ag-Cu nanoalloys: an electrochemical sensor for H_2O_2 detection. Surf Interfaces 36:102616
18. Gholami M, Koivisto B (2019) A flexible and highly selective non-enzymatic H_2O_2 sensor based on silver nanoparticles embedded into Nafion. Appl Surf Sci 467-468:112–118
19. Han J, Zeng H-Y, Cao X, Chen C-R (2017) Cycling stability of iron-based layered double hydroxide thin-films for battery-type electrode materials. J Mater Sci Mater Electron 28(3):2754–2762
20. Yuan J, Xu S, Zeng H-Y, Cao X, Pan A-DG-F, Xiao D, P.-X. (2018) Hydrogen peroxide biosensor based on chitosan/2D layered double hydroxide composite for the determination of H_2O_2. Bioelectrochemistry 123:94–102
21. Zhao S, Yi H, Tang X, Kang D, Gao F, Wang J, Huang Y, Yang Z (2018) Removal of volatile odorous organic compounds over NiAl mixed oxides at low temperature. J Hazard Mater 344:797–810
22. Yin J, Qi X, Yang L, Hao G, Li J, Zhong J (2011) A hydrogen peroxide electrochemical sensor based on silver nanoparticles decorated silicon nanowire arrays. Electrochim Acta 56(11):3884–3889
23. Sharma RK, Rastogi AC, Desu SB (2008) Manganese oxide embedded polypyrrole nanocomposites for electrochemical supercapacitor. Electrochim Acta 53(26):7690–7695
24. Zhang K, Zeng H-Y, Wang M-X, Li H-B, Yan W, Wang H-B, Tang Z-H (2022) 3D hierarchical core-shell structural NiCoMoS@NiCoAl hydrotalcite for high-performance supercapacitors. J Mater Chem A 10(20):11213–11224
25. Huo Y, Wang Z, Zhang J, Liang C, Dai K (2018) Ag SPR-promoted 2D porous g-C_3N_4/Ag_2MoO_4 composites for enhanced photocatalytic performance towards methylene blue degradation. Appl Surf Sci 459:271–280
26. Cao S, Li Y, Tang Y, Sun Y, Li W, Guo X, Yang F, Zhang G, Zhou H, Liu Z, Li Q, Shakouri M, Pang H (2023) Space-confined metal ion strategy for carbon materials derived from cobalt benzimidazole frameworks with high desalination performance in simulated seawater. Adv Mater:2301011
27. Yi T-F, Qiu L-Y, Mei J, Qi S-Y, Cui P, Luo S, Zhu Y-R, Xie Y, He Y-B (2020) Porous spherical NiO@$NiMoO_4$@PPy nanoarchitectures as advanced electrochemical pseudocapacitor materials. Sci Bull 65(7):546–556
28. Shishegari N, Sabahi A, Manteghi F, Ghaffarinejad A, Tehrani Z (2020) Non-enzymatic sensor based on nitrogen-doped graphene modified with Pd nano-particles and NiAl layered double

hydroxide for glucose determination in blood. J Electroanal Chem 871:114285
29. Wang GX, Yang L, Chen Y, Wang JZ, Bewlay S, Liu HK (2005) An investigation of polypyrrole-$LiFePO_4$ composite cathode materials for lithium-ion batteries. Electrochim Acta 50(24):4649–4654
30. Yan W, Zeng H-Y, Zhang K, Long Y-W, Wang M-X (2023) Ni-Co-Mn hydrotalcite-derived hierarchically porous sulfide for hybrid supercapacitors. J Colloid Interface Sci 635:379–390
31. Wang Q, Zheng J (2010) Electrodeposition of silver nanoparticles on a zinc oxide film: improvement of amperometric sensing sensitivity and stability for hydrogen peroxide determination. Microchim Acta 169(3):361–365
32. Aparicio-Martínez E, Ibarra A, Estrada-Moreno IA, Osuna V, Dominguez RB (2019) Flexible electrochemical sensor based on laser scribed graphene/Ag nanoparticles for non-enzymatic hydrogen peroxide detection. Sensors Actuators B Chem 301:127101
33. Li W, Liu J, Chen C, Zhu Y, Liu N, Zhou Y, Chen S (2022) High catalytic performance non-enzymatic H_2O_2 sensor based on $Cu_2O@Cu_9S_5$ yolk-shell nanospheres. Appl Surf Sci 587:152766
34. Zhang Y, Wang Q, Liu D, Wang Q, Li T, Wang Z (2020) Cu_2O-BiOI isotype (p-p) heterojunction: boosted visible-light-driven photoelectrochemical activity for non-enzymatic H_2O_2 sensing. Appl Surf Sci 521:146434
35. Li Y, Tang L, Deng D, Ye J, Wu Z, Wang J, Luo L (2019) A novel non-enzymatic H_2O_2 sensor using $ZnMn_2O_4$ microspheres modified glassy carbon electrode. Colloids Surf B Biointerfaces 179:293–298
36. Sheng ZM, Gan ZZ, Huang H, Niu RL, Han ZW, Jia RP (2020) M-Nx (M = Fe, Co, Ni, Cu) doped graphitic nanocages with high specific surface area for non-enzymatic electrochemical detection of H_2O_2. Sensors Actuators B Chem 305:127550
37. Carbone M, Aneggi E, Figueredo F, Susmel S (2022) NiO-nanoflowers decorating a plastic electrode for the non-enzymatic amperometric detection of H_2O_2 in milk: old issue, new challenge. Food Control 132:108549